This document is the unedited Author's version of a Submitted Work that was subsequently accepted for publication in The Journal of Physical Chemistry Letters, copyright © American Chemical Society after peer review. To access the final edited and published work see https://doi.org/10.1021/acs.jpclett.1c00600" http://pubs.acs.org/paragonplus/copyright/jpa_form_a.pdf . Access to this work was provided by the University of Maryland, Baltimore County (UMBC) ScholarWorks@UMBC digital repository on the Maryland Shared Open Access (MD-SOAR) platform.

Please provide feedback Please support the ScholarWorks@UMBC repository by emailing scholarworks-group@umbc.edu and telling us what having access to this work means to you and why it's important to you. Thank you.

Viscoelasticity enhances nanometer-scale slip in gigahertz-frequency liquid flows

Debadi Chakraborty,[1,†] Brian Uthe,[2,†] Edward W. Malachosky,[3]

Matthew Pelton[2,] and John E. Sader[1,‡]*

[1] ARC Centre of Excellence in Exciton Science, School of Mathematics and Statistics, The University of Melbourne, Victoria 3010, Australia

[2] Department of Physics, UMBC (University of Maryland, Baltimore County), Baltimore, MD 21250, USA

[3] James Franck Institute, University of Chicago, Chicago, IL 60637, USA

†Equal contribution

** mpelton@umbc.edu*

‡ jsader@unimelb.edu.au

Abstract

The interaction between flowing liquids and solid surfaces underpins many physical phenomena and technologies, such as the ability of an airfoil to generate lift and the mixing of liquids for industrial applications. These phenomena are often described using the Navier Stokes equations and the no-slip boundary condition: the assumption that the liquid immediately adjacent to a solid surface does not move relative to the surface. Here, we observe violation of the no-slip condition with strong enhancement of slip due to intrinsic viscoelasticity of the bulk liquid. This is achieved by measuring the 20-GHz acoustic vibrations of gold nanoparticles in glycerol/water mixtures, for which the underlying physics is explored using rigorous, theoretical models. The reported enhancement of slip revises current understanding of ultrafast liquid flows, with implications for technologies ranging from membrane filtration to nanofluidic devices and biomolecular sensing.

The no-slip condition is a central tenant of continuum fluid mechanics [1, 2]. It has been the subject of constant investigation since it was first proposed in the 19th century, having been adopted on empirical grounds [3]. Since that time, an array of natural phenomena has been found to be inconsistent with its direct application [4]. Perhaps most striking amongst these exceptions is the moving three-phase contact line [5], such as the interface between a solid object and the air-water surface, which is commonly encountered in everyday settings. The resulting paradox that no-slip gives no motion of the solid object can be alleviated through use of the alternate Navier slip condition—where the relative velocity of the solid and liquid is proportional to the strain rate of the liquid. Use of the Navier slip condition is supported by molecular dynamics simulations [6-9] and arguments from linear response theory; it has also been suggested that liquid slip can be modelled as a kinetic rate process [10].

These molecular simulations predict slip lengths between solid surfaces and wetting liquids at the single-nanometer scale [9]. Slip thus has the potential to be of critical importance for a range of emerging technologies, including membrane filtration and separation [11, 12], hydraulic fracturing [13], lab-on-chip systems [14, 15], and mass-based sensing of biomolecules [16]. A number of experimental observations have also been made that are consistent with sub-micrometer slip lengths at liquid-solid interfaces; for example, nearly frictionless flow has been observed through carbon nanotubes and other nanoscale channels [17-19]. Here, we augment this current understanding of slip flows in liquid by showing that bulk molecular relaxation processes inherent to simple liquids at short time scales [20-24], i.e., the intrinsic viscoelasticity of liquids, drastically amplify slip. This

discovery is expected to impact a host of technologies, providing an additional handle on controlling liquid flows at nanometer scales.

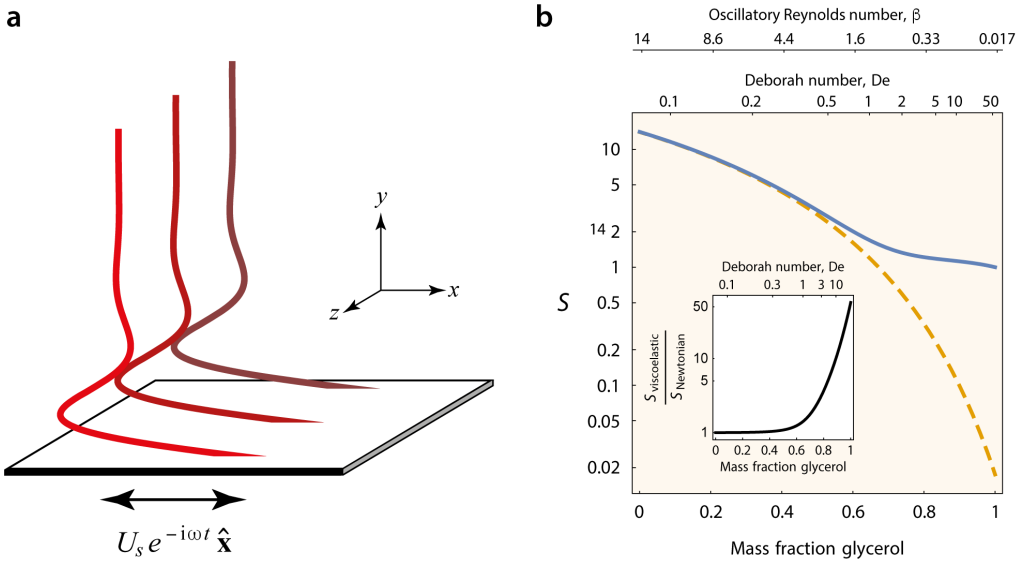

Figure 1. Sensitivity, S, of the quality factor of a cylindrical nanoparticle to slip, as defined in Eq. (7). a, Schematic of Stokes 2nd problem used to formulate the mathematical model for S. The oscillating plate generates diffusive shear waves that emanate from the plate into the fluid. The Cartesian coordinate system is indicated; the origin of this coordinate system is taken to be on the surface of the plate. The plate is flat and spatially infinite in extent, with an unbounded and quiescent fluid in the region, $y \geq 0$. b, Plot of S vs mass fraction glycerol for a circular cylinder undergoing extensional vibration in glycerol/water mixtures. Nanoparticle dimensions: 80 nm long and 20 nm diameter. Resonant frequency: 20 GHz. Viscoelastic properties of glycerol/water mixtures are taken from Refs. 20 and 23, at 25 °C. Upper (blue) curve is viscoelastic flow according to Eq. (7), while lower (orange) is Newtonian result (De $= 0$, provided for reference). The inset shows the ratio of S to its value in the limit of Newtonian behavior.

We theoretically model the combined effects of bulk viscoelasticity and surface slip using a single relaxation time Maxwell model for the liquid [25, 26],

$$\mathbf{T} = -p\mathbf{I} + \mathbf{S}, \qquad \mathbf{S} + \lambda \frac{\partial \mathbf{S}}{\partial t} = 2\mu \mathbf{e}, \tag{1}$$

where $\mathbf{T}$ is the stress tensor, $\mathbf{I}$ is the identity tensor, p is the pressure, $\mathbf{S}$ is the deviatoric stress tensor, $\mathbf{e} = 1/2(\nabla \mathbf{u} + (\nabla \mathbf{u})^{\mathrm{T}})$ is the rate-of-strain tensor, $\mathbf{u}$ is the liquid velocity field, t is time, and μ is the liquid's shear viscosity. The Navier slip condition is invoked at the solid surface [27, 28],

$$[(\mathbf{u} - \mathbf{u}_s - 2b\, \mathbf{n} \cdot \mathbf{e}) \cdot (\mathbf{I} - \mathbf{nn})]_{\text{surface}} = \mathbf{0}, \tag{2}$$

where $\mathbf{n}$ is the unit normal to the surface, $\mathbf{u}_s$ is the solid velocity field, and b is the (constant) slip length, a constitutive property of the solid-liquid interface. Equations (1) and (2) are combined with Cauchy's equation of motion for the liquid and Navier's equation for the solid deformation to define a complete and self-consistent theory for the fluid-structure interaction of a nanoparticle vibrating in liquid [20, 29]. Characterizing the dynamics of these particles in liquid is the principal focus of this study.

As a first step, we calculate the shear flow generated by a solid plate at the Cartesian position, $y = 0$ (Figure 1a), that is oscillating with velocity $U_s e^{-\mathrm{i}\omega t}\hat{\mathbf{x}}$, where ω is the oscillation frequency, i is the imaginary unit, and $\hat{\mathbf{x}}$ is the unit vector in the x-direction and is parallel to the plate. The solid plate is in contact with the viscoelastic liquid occupying the half space, $y \geq 0$, whose velocity field is calculated using the above-mentioned theory and found to be

$$\mathbf{u}(y,t) = U_s \frac{\exp\left(-C\frac{y}{\delta}\right)}{1+\frac{b}{\delta}C} e^{-\mathrm{i}\omega t}\hat{\mathbf{x}}\,, \tag{3}$$

where the (Newtonian) viscous penetration depth, $\delta = \sqrt{\mu/(\rho\omega)}$, is proportional to the length scale over which the flow varies in the viscous limit, and ρ is the liquid density.

Equation (3) shows that this penetration depth—which defines the hydrodynamic length scale—is reduced in a viscoelastic Maxwell fluid by the elastic coefficient,

$$C = (1 + \mathrm{De}^2)^{\frac{1}{4}}\, e^{-\mathrm{i}\left(\frac{\pi}{4} + \frac{1}{2}\arctan \mathrm{De}\right)}, \tag{4}$$

where the Deborah number, $\mathrm{De} = \omega\lambda$, specifies the importance of viscoelastic effects in the liquid [25]; $\mathrm{De} = 0$ corresponds to a Newtonian liquid, while $\mathrm{De} \to \infty$ is the elastic limit. Because velocity slip at the surface is proportional to the velocity gradient in the liquid, this reduction in the penetration depth due to viscoelasticity (finite De) increases velocity slip at the solid-liquid interface for a given slip length, b; see Eq. (3) for $y = 0$.

Next, we use Eq. (3) to calculate the quality factor, Q, i.e., the scaled ratio of elastic energy relative to damping, for a slender elastic circular cylinder of radius R and density ρ_s in a viscoelastic fluid of density, ρ; Eq. (3) specifies the fluid stress at the cylinder walls. Assuming a heavy cylinder relative to the surrounding liquid, i.e., $\rho_s \gg \rho$, gives the following formulas in the Newtonian and elastic regimes,

$$Q = \hat{\rho}\sqrt{\frac{\beta}{2}} \begin{cases} 1 + \dfrac{\Delta\,\beta}{1 + \sqrt{2\,\Delta\,\beta}} & , \mathrm{De} = 0 \\ \sqrt{\dfrac{\mathrm{De}}{2}}\,(1 + \Delta\,\mathrm{De}\,\beta) & , \mathrm{De} \to \infty \end{cases}, \tag{5}$$

where the oscillatory Reynolds number (dimensionless frequency), $\beta = (R/\delta)^2$, the squared dimensionless slip length, $\Delta = (b/R)^2$, the density ratio, $\hat{\rho} = \rho_s/\rho$, and ω is evaluated at ω_{vac}, the cylinder's resonant frequency in vacuum. This analytical calculation implicitly assumes that the viscous penetration depth, δ, is far smaller than the cylinder radius, R, a restriction invoked here for analytical simplicity which we relax later in this study. The corresponding general expression for arbitrary De, to leading order in small Δ (the practical case), is

$$Q = \tfrac{1}{2}\hat{\rho}\sqrt{\beta}\left(1 + \Delta\,\beta\,\sqrt{1+\mathrm{De}^2}\right)(1+\mathrm{De}^2)^{\frac{1}{4}}\csc\left(\frac{\pi}{4}+\frac{1}{2}\arctan\mathrm{De}\right) + o(\Delta), \tag{6}$$

from which the relative sensitivity of the quality factor to the slip length follows:

$$S \equiv \frac{1}{Q}\frac{dQ}{d\Delta}\bigg|_{\Delta=0} = \beta\sqrt{1+\mathrm{De}^2}. \tag{7}$$

In Eq. (7), the term β is the Newtonian component of the sensitivity, and $\sqrt{1+\mathrm{De}^2}$ is the enhancement factor due to viscoelasticity. The enhancement factor increases monotonically with De, showing that the sensitivity of the quality factor to the slip length can increase drastically through the action of liquid viscoelasticity. Figure 1b gives numerical results for the sensitivity for a cylindrical nanoparticle undergoing extensional vibrations at 20 GHz in a range of glycerol/water mixtures. The initial decrease in S with increasing glycerol mass fraction is due to enhanced viscosity, while the plateau at large mass fraction arises from viscoelasticity. Enhancement in S due to the action of viscoelasticity, i.e., nonzero De compared to $\mathrm{De} = 0$, can exceed a factor of 50 for pure glycerol; see inset of Figure 1b. This analysis assumes a constant slip length, b, as a function of glycerol mass fraction, which is consistent with the measurements that we report below.

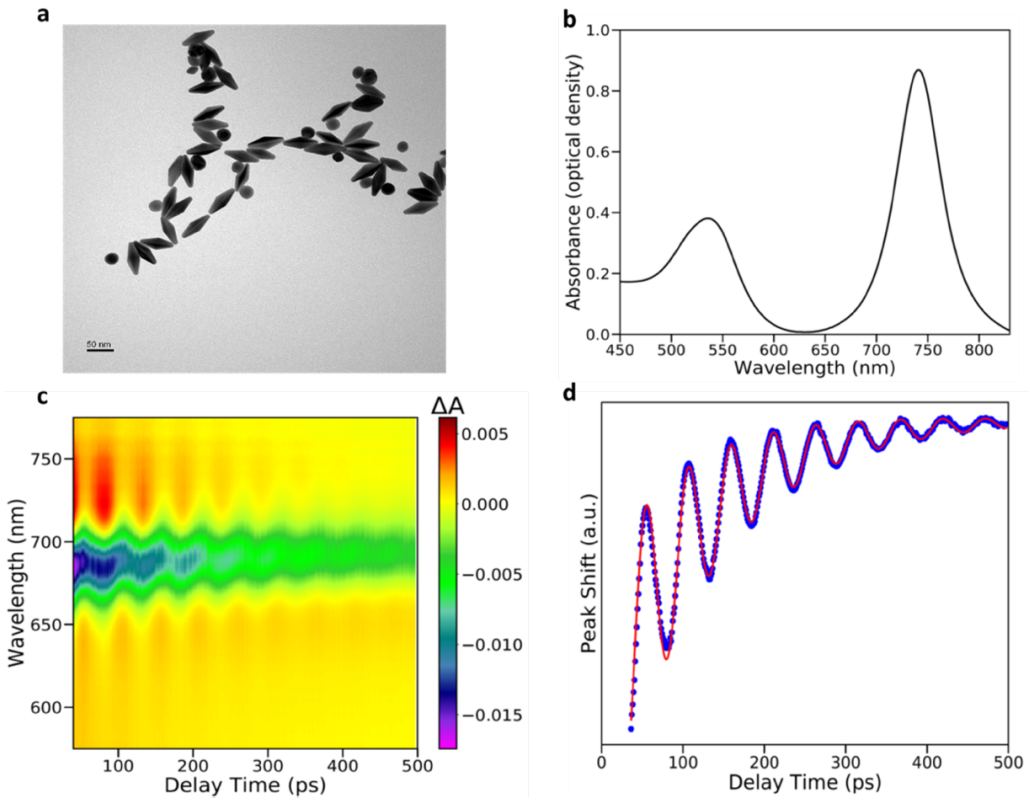

Figure 2. Vibration of gold bipyramidal nanoparticles. (a) Transmission electron microscope image of gold bipyramids and spheroidal byproduct; see Materials and methods for details. (b) Linear extinction spectrum for an ensemble of gold bipyramids suspended in water. The narrow peak centered approximately at 745 nm corresponds to the longitudinal plasmon resonance of the bipyramids. The broader peak centered approximately at 540 nm corresponds primarily to the plasmon resonance of the spheroidal biproduct. (c) Extinction change after excitation by an initial pump laser pulse tuned to the longitudinal plasmon resonance of the bipyramidal sample as a function of probe pulse wavelength and delay time between the arrival of the pump pulse and probe pulse. (d) Change in the peak plasmon resonance frequency, blue dots, obtained from fitting the data in (c). The red line is a fit to the corresponding peak shifts using a model of a damped oscillation on top of a decaying background.

To experimentally investigate this theoretically predicted enhancement of surface slip by viscoelasticity of the bulk liquid, we probe the dynamic response of metal nanoparticles immersed in glycerol/water mixtures with different compositions and at different temperatures. Bipyramidal gold nanoparticles capped with polystyrene sulfonic acid (PSS) are used [20, 30]. A representative transmission-electron microscope (TEM) image of the nanoparticles is given in Figure 2a, and their extinction spectrum in water is shown in Figure 2b. The bipyramidal particles have a different geometry from the idealized circular cylinder studied above; the latter was chosen for simplicity of mathematical analysis. The frequency and decay rate for vibrations of the nanoparticles are measured using transient-absorption spectroscopy [31, 32]; see Materials and methods, and the representative dataset in Figure 2c-d. The nanoparticles resonate at a frequency of ≈20 GHz which is insensitive to the liquid of immersion [20].

Figure 3 gives the measured quality factors for the bipyramidal nanoparticles immersed in a glycerol/water mixture with 20% glycerol mass fraction, as a function of temperature. The Deborah number, De, is small, and the liquid behaves in a Newtonian fashion. Increasing the temperature reduces the shear viscosity of the liquid, which increases Q. This experimental dataset is compared to finite-element (FE) simulations of the complete theory for the fluid-structure problem (see discussion after Eq. (2)), implemented as in Ref. 10 but with a Navier slip condition. This numerical approach eliminates any restriction imposed by the analytical model (discussed above) and provides an accurate solution to the complete theory for the experimental system.

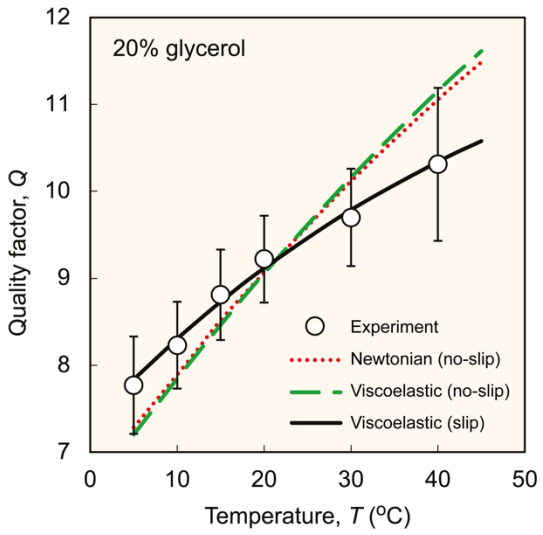

Figure 3. Quality factor for vibrations of bipyramidal gold nanoparticles in a glycerol/water mixture containing 20% mass fraction glycerol. Comparison of measurement and three theories: (i) Newtonian liquid with no-slip boundary condition, (ii) viscoelastic liquid with no-slip boundary condition, (iii) viscoelastic liquid with a Navier slip length of 3.7 ± 0.4 nm (SE). The intrinsic quality factor, Q_{int}, is varied for each model to minimize the mean square difference between theory and measured data [20, 29, 33, 34]; fitted values are 27 for the Newtonian model, 29 for the viscoelastic model without slip, and 14.5 for the viscoelastic model with slip. Errors bars represent 95% confidence intervals.

The first set of theoretical results in Figure 3 assume Newtonian behavior with no-slip, which is fit to the measured data by adjusting the intrinsic quality factor (not known *a priori* [20, 29, 33, 34]). Identical quantitative behavior is observed for the second theory that includes the viscoelastic properties of the liquid, because the Deborah number is small for these measurements. These no-slip theories give rates-of-change in the quality factor with respect to temperature, T, that are much larger ($\approx$50%) than observed. A complementary analysis using the no-slip condition is given in Supplementary Information Figure 1 for

measurements at different but fixed temperatures, where the glycerol mass fraction is now varied. The same conclusion results: use of no-slip does not explain the measurements.

The third theory used in Figure 3 involves replacing the no-slip condition in the second (viscoelastic) theory with the Navier slip condition, Eq. (2) [36]; low De ensures that all flows at 20% glycerol mass fraction are Newtonian in nature. Adjusting both the slip length and intrinsic quality factor to minimize the mean square difference between theory and measurement yields a slip length of $b = 3.7 \pm 0.4$ nm (SE). In contrast to the no-slip theories above, this fit delivers a remarkable match across the entire measurement dataset, thereby providing strong evidence for the presence of slip at the liquid-nanoparticle interface.

Figure 4 compares FE simulations to measurements at higher glycerol mass fraction (60 – 80%). A marked difference between the Newtonian and viscoelastic models arises here, due to the higher Deborah numbers of these measurements. The Newtonian model is strictly not applicable due to the effects of viscoelasticity; the Newtonian no-slip result is shown for reference only. Strikingly, the viscoelastic model with a single slip length, $b = 3.7$ nm—obtained independently from Figure 3 for 20% glycerol only—gives excellent agreement with measurements for all higher glycerol mass fractions. Similarly, the intrinsic quality factor obtained from the 20% glycerol measurement is used throughout. A complementary analysis at fixed temperature, using the same viscoelastic model and the same slip length of 3.7 nm, also yields excellent agreement with all measurements at these high glycerol concentrations; see Supplementary Information Figure 2. No-slip does not describe these measurements, nor does the Newtonian model which becomes less sensitive to slip with increasing viscosity (i.e., higher glycerol mass fraction). In contrast, the viscoelastic model exhibits a near constant sensitivity to slip for all glycerol mass fractions and temperatures,

as viscosity varies by a factor of 40. As shown in Figure 4, the model also displays excellent agreement with measurement. The results in Figure 4 thus highlight the drastic amplification of slip that viscoelasticity of the liquid provides and the importance of slip in these flows.

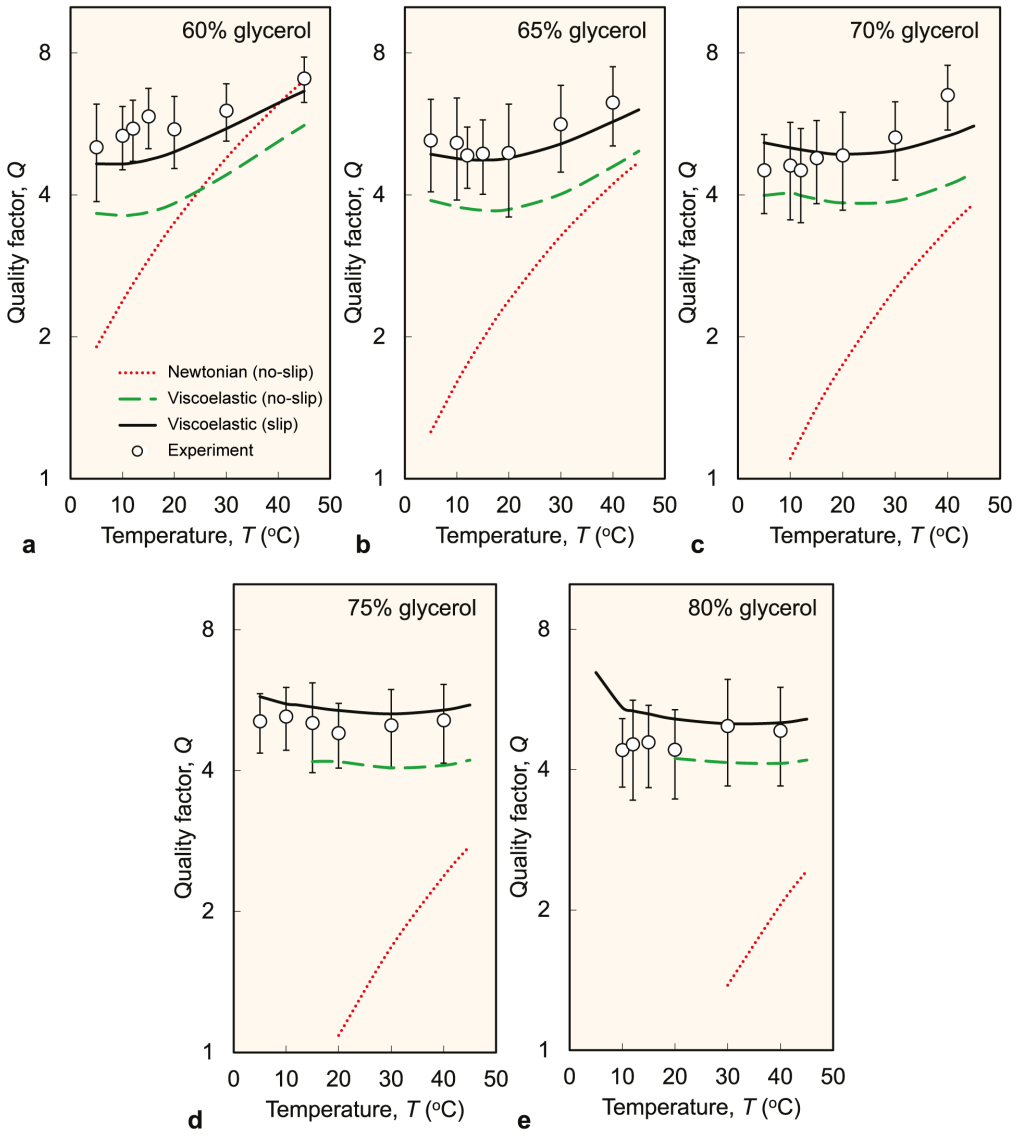

Figure 4. Quality factor for vibrations of bipyramidal gold nanoparticles in glycerol/water mixtures of varying glycerol mass fraction. (a) 60% glycerol; (b) 65% glycerol; (c) 70% glycerol; (d) 75% glycerol; (e) 80% glycerol. Experimental flows are viscoelastic with the Newtonian model strongly underestimating the measured quality factors. The slip lengths and intrinsic quality factors in the

theoretical models are identical to those used in Figure 3 (for 20% glycerol). Errors bars represent 95% confidence intervals.

In summary, this study demonstrates that gold nanoparticles executing gigahertz vibrations in simple liquids exhibit a strong sensitivity to slip at the solid surface. This sensitivity arises because the vibrational frequency of the nanoparticles accesses bulk viscoelastic processes of the liquids. Use of a single slip length of 3.7 ± 0.4 nm (SE) with a viscoelastic Maxwell model yields excellent agreement with all measurements of bipyramidal gold nanoparticles immersed in a wide range of glycerol/water mixtures and temperatures. The slip length should depend on the nature of the liquid-solid interaction [9] with the dependence on material properties, capping layers and other environmental conditions defining an interesting direction for future study.

The interplay that we study between surface slip and bulk viscoelasticity is qualitatively different from effects previously studied in complex fluids, which can arise from molecular entanglement and phase separation [36, 37]. Our study shows that theoretical treatments of slip for inherently high-frequency liquid flows must generally consider bulk viscoelastic processes in the liquid to approach quantitative correctness. Our findings will thus impact technologies that involve the ultrafast flow of simple liquids at nanometer length scales [11-16].

Materials and methods

Sample synthesis and preparation

Gold bipyramids are synthesized by a seed-mediated procedure, following Refs. 30 and 38. First, gold seeds are synthesized by mixing 250 μL of a gold chloride solution with 500

μL of a sodium citrate solution and 300 μL of a fresh sodium borohydride solution in 18.95 mL of nanopure water (NPH_2O) at room temperature under vigorous stirring for 2 hours. Gold bipyramids are then synthesized by dissolving 364 mg of CTAB in 10 mL of NPH_2O at 30 °C under vigorous stirring, then adding 500 μL of a 10 mM gold chloride solution, 100 μL of a 10 mM silver nitrate solution, 200 μL of a 1 M HCl solution, 80 μL of a 100 mM vitamin C solution, and 120 μL of the gold seed solution. The colloid is allowed to react for two hours. After the synthesis, the gold bipyramids are centrifuged at 8500 g and 30 °C for 30 minutes. The supernatant is then decanted and the pellet resuspended with 2 mL of NPH_2O.

After the synthesis, the gold bipyramids are functionalized with polystyrene sulfonic acid (PSS), following Ref. 20. This bipyramid solution is centrifuged for 30 minutes at 8500 g and 30 °C. Again, the supernatant is decanted and the pellet resuspended with 2 mL of NPH_2O. The cleaned colloid is divided into 6 aliquots, diluted to a final volume of 1.5 mL with NPH_2O, and then centrifuged at 5000 *g* for 10 to 20 minutes. The supernatants are decanted, and the pellets resuspended with 1 mL of NPH_2O and 500 μL of a 0.1% wt PSS solution. The solutions are vigorously mixed, soaked for 4 hours, and centrifuged at 5000 g for 15 to 25 minutes. The supernatants are then decanted and the pellets are resuspended with 1 mL of NPH_2O each. The structure of the particles is verified by transmission-electron-microscope imaging using a FEI Spirit TEM with an operating voltage of 120 kV, and their optical properties are verified by measuring absorption spectra using an HP/Agilent 6453 UV/Vis spectrometer.

The solutions for the optical measurements are formed by mixing small volumes of the PSS-functionalized nanoparticles with different mass concentrations of water and glycerol,

such that the optical density of the longitudinal plasmon resonance of the solution contained in a 2-mm cuvette is between 0.25 and 0.35.

The bipyramids have a narrow size distribution, with less than 3 nm standard deviation in their lengths. This results in a narrow range of vibrational frequencies, so that decay of their vibrations is dominated by energy damping rather than inhomogeneous dephasing. A spheroidal gold-nanoparticle byproduct is also produced during the bipyramid synthesis; however, this byproduct has a plasmon resonance centered at 540 nm, well separated from the longitudinal-plasmon resonance of the bipyramids at 745 nm; see Figure 2b. This separation in wavelength allows for optical measurements to probe only the gold bipyramids.

Transient-absorption measurements and data analysis

Measurements are performed following Refs. 20, 33 and 34. A suspension of bipyramidal gold nanoparticles is excited with a pump laser tuned to their longitudinal plasmon resonance. Absorption of pump laser light by the bipyramids leads to their rapid heating and expansion; this, in turn, impulsively excites coherent acoustic oscillations of the nanoparticles. The resulting periodic changes in the shape and size of the nanoparticles, as well as varying strain within the nanoparticles, all result in oscillation of the longitudinal plasmon frequency. This oscillation is detected through the changes it produces in the transmission of a time-delayed probe pulse. The frequency and decay rate of the oscillating signal give the quality factor for the nanoparticle vibrations.

Measurements are performed using an Ultrafast Systems Helios spectrometer. Pump and probe laser pulses are derived from a regeneratively amplified Ti:Sapphire oscillator

(Spectra Physics Tsunami/SpitfirePro) operating at 2 kHz. A 90:10 beam splitter is then used to create the pump pulse (90%) and the probe pulse (10%) from the amplifier output. The probe pulse travels along a path with a delay line to control when it arrives at the sample in relation to the pump pulse. Before the sample, the probe pulse passes through a sapphire plate to generate a continuum, which is then focused to a point inside the sample cuvette. The transmitted light is coupled into an optical fiber and passed to a spectrometer.

Approximately 5 spectra at negative pump-probe laser pulse delay times, corresponding to the probe pulse arriving before the pump pulse, are averaged and subtracted from all remaining spectra. The corrected transient extinction spectra are fitted, for each time delay, to a difference of Lorentzian functions using a non-linear least squares technique. This is used to determine the plasmon resonance peak position at each delay time. From this, the fractional peak shift as a function of time is fitted to a model of a damped oscillation on a decaying background using the same non-linear least squares fitting routine. We begin the fit at a delay time of 35 ps to ensure that changes in the spectra are a result only of the vibrations of the nanoparticle.

The fitted decay time and oscillation frequency are dependent on the incident pump power, and an orthogonal distance regression linear extrapolation is performed to obtain values for zero incident pump power. The resulting zero-power decay times result from a combination of inhomogeneous dephasing due to the size variation of the nanoparticle sample and homogeneous viscous damping by the fluid. The inhomogeneous contribution is subtracted from the overall decay time using the distribution of lengths determined from TEM images of the sample. The resulting energy decay times are used to determine the quality factors.

Acknowledgments

The authors thank Philippe Guyot-Sionnest for supervision of nanoparticle synthesis and Adam Goad for assistance with transient-absorption measurements. M.P. and B.U. acknowledge funding from the U.S. National Science Foundation under grant DMR-1554895. D.C. and J.E.S. gratefully acknowledge support from the Australian Research Council Centre of Excellence in Exciton Science (CE170100026) and the Australian Research Council Grants Scheme.

Author contributions

J.E.S. and M.P. supervised the project and conceived the measurements. B.U. performed the measurements. D.C. analyzed the resulting dataset, performed FE simulations, and proposed that the results constituted evidence for slip. J.E.S. and D.C. developed supporting theory. E.W.M. synthesized and functionalized nanoparticle samples. All authors contributed to discussions and to writing of the manuscript.

Conflicts of interest

There are no conflicts to declare.

References

1. S. Goldstein, *Modern Developments in Fluid Dynamics* (Oxford Univ. Press, Oxford, 1938)
2. S. Goldstein, Fluid mechanics in the first half of this century. *Annu. Rev. Fluid Mech.,* 1969, **1,** 1-28.

3. G. G. Stokes, *Mathematical and Physical Papers: On the Theories of the Internal Friction of Fluids in Motion, and of the Equilibrium and Motion of Elastic Solids* (Cambridge Univ. Press, Cambridge, 1901).

4. C. Neto, D. R. Evans, E. Bonaccurso, H. J. Butt and V. S. J. Craig, Boundary slip in Newtonian liquids: a review of experimental studies. *Rep. Prog. Phys.,* 2005, **68,** 2859-2897.

5. J. H. Snoeijer and B. Andreotti, Moving contact lines: scales, regimes, and dynamical transitions. *Annu. Rev. Fluid Mech.,* 2013, **45,** 269-292.

6. P. A. Thompson and S. M. Troian, A general boundary condition for liquid flow at solid surfaces. *Nature*, 1997, **389,** 360-362.

7. J. L. Barrat and L. Bocquet, Large slip effect at a nonwetting fluid-solid interface. *Phys. Rev. Lett.,* 1999, **82,** 4671-4674.

8. M. Cieplak, J. Koplik and J. R. Banavar, Boundary conditions at a fluid-solid interface. *Phys. Rev. Lett.,* 2001, **86,** 803-806.

9. D. M. Huang, C. Sendner, D. Horinek, R. R. Netz and L. Bocquet, Water slippage versus contact angle: a quasiuniversal relationship. *Phys. Rev. Lett.,* 2008, **101,** 226101.

10. G. J. Wang and N. G. Hadjiconstantinou, Universal molecular-kinetic scaling relation for slip of a simple fluid at a solid boundary. *Phys. Rev. Fluids,* 2019, **4,** 064201.

11. R. R. Nair, *et al.*, Unimpeded permeation of water through helium-leak–tight graphene-based membranes. *Science,* 2012, **335,** 442-444.

12. L. Wang, *et al.*, Fundamental transport mechanisms, fabrication and potential applications of nanoporous atomically thin membranes. *Nat. Nanotechnol.,* 2017, **12,** 509-522.

13. F. Javadpour, M. McClure and M. E. Naraghi, Slip-corrected liquid permeability and its effect on hydraulic fracturing and fluid loss in shale. *Fuel,* 2015, **160,** 549-559.

14. H. A. Stone, A. D. Stroock and A. Ajdari, Engineering flows in small devices: microfluidics toward a lab-on-a-chip. *Annu. Rev. Fluid Mech.,* 2004, **36,** 381-411.

15. P. A. Tabeling, Brief introduction to slippage, droplets and mixing in microfluidic systems. *Lab Chip,* 2009, **9,** 2428-2436.

16. T. P. Burg, *et al.,* Weighing of biomolecules, single cells and single nanoparticles in fluid. *Nature,* 2007, **446,** 1066-1069.

17. M. Majumder, N. Chopra, R. Andrews and B. J. Hinds, Enhanced flow in carbon nanotubes. *Nature,* 2005, **438,** 44-44.

18. J. K. Holt, *et al.,* Fast mass transport through sub-2-nanometer carbon nanotubes. *Science,* 2006, **312,** 1034-1037.

19. E. Secchi, *et al.,* Massive radius-dependent flow slippage in carbon nanotubes. *Nature,* 2016, **537,** 210-213.

20. M. Pelton, D. Chakraborty, E. W. Malachosky, P. Guyot-Sionnest and J. E. Sader, Viscoelastic flows in simple liquids generated by vibrating nanostructures. *Phys. Rev. Lett*., 2013, **111,** 244502.

21. D. Chakraborty, G. V. Hartland, M. Pelton and J. E. Sader, When can the elastic properties of simple liquids be probed using high-frequency nanoparticle vibrations? *J. Phys. Chem. C,* 2018, **122,** 13347-13353.

22. T. Devkota, *et al.,* On the measurement of relaxation times of acoustic vibrations in metal nanowires. *Phys. Chem. Chem. Phys.,* 2018, **20,** 17687-17693.

23. W. M. Slie, A. R. Donfor and T. A. Litovitz, Ultrasonic shear and longitudinal measurements in aqueous glycerol. *J. Chem. Phys.,* 1966, **44**, 3712-3718.

24. C. Klieber, V. E. Gusev, T. Pezeril and K. A. Nelson, Nonlinear acoustics at GHz frequencies in a viscoelastic fragile glass former. *Phys. Rev. Lett*., 2015, **114,** 065701.

25. W. R. Schowalter, *Mechanics of Non-Newtonian Fluids* (Pergamon, Oxford, 1978).

26. D. Chakraborty and J. E. Sader, Constitutive models for linear compressible viscoelastic flows of simple liquids at nanometer length scales. *Phys. Fluids,* 2015, **27,** 052002.

27. J. C. Maxwell, On stresses in rarefied gases arising from inequalities of temperature. *Phil. Trans. R. Soc*., 1879, **170,** 231-256.

28. W. G. Vincenti and C. H. J. Kruger, *Introduction to Physical Gas Dynamics* (Krieger, New York, 1967).

29. D. Chakraborty, E. van Leeuwen, M. Pelton and J. E. Sader, Vibration of nanoparticles in viscous fluids. *J. Phys. Chem. C,* 2013, **117,** 8536-8544.

30. M. Liu and P. Guyot-Sionnest, Mechanism of silver(I)-assisted growth of gold nanorods and bipyramids. *J. Phys. Chem. B,* 2005, **109,** 22192-22200.

31. G. V. Hartland, Optical studies of dynamics in noble metal nanostructures. *Chem. Rev.,* 2011, **111,** 3858-3887.

32. A. Ahmed, M. Pelton and J. R. Guest, Understanding how acoustic vibrations modulate the optical response of plasmonic metal nanoparticles. *ACS Nano,* 2017, **11,** 9360-9369.

33. M. Pelton, *et al.*, D. Damping of acoustic vibrations in gold nanoparticles. *Nat. Nanotechnol.,* 2009, **4,** 492-495.

34. M. Pelton, Y. Wang, D. Gosztola and J. E. Sader, Mechanical damping of longitudinal acoustic oscillations of metal nanoparticles in solution. *J. Phys. Chem. C,* 2011, **115**, 23732-23740.

35. The idealized model for a cylindrical nanoparticle of zero radius-to-length ratio, Eq. (5), gives a quadratic dependence on slip length, b, while FE simulations of the (measured) bipyramidal particles produces a linear dependence. The observed linear dependence on b is likely due to

the axially varying cross section of the bipyramids and end effects that are not considered in the analytical model.

36. L. Léger, H. Hervet, G. Massey and E. Durliat, Wall slip in polymer melts. *J. Condens. Matter Phys.,* 1997, **9,** 7719-7740.

37. H. A. Barnes, A review of the slip (wall depletion) of polymer solutions, emulsions and particle suspensions in viscometers: its cause, character, and cure. *J. Non Newton. Fluid Mech.,* 1995, **56,** 221-251.

38. N. Jana, L. Gearheart and C. Murphy, Wet chemical synthesis of high aspect ratio cylindrical gold nanorods, *J. Phys. Chem. B,* 2001, **105,** 4065-4067.